INTERFACE SCIENCE 12, 259–266, 2004

Analysis of Bulk and Interface Phenomena in CdTe/CdS Thin-Film Solar Cells

M. TERHEGGEN,* H. HEINRICH AND G. KOSTORZ
ETH Zurich, Institute of Applied Physics, CH-8093 Zurich, Switzerland
mathias_terheggen@mckinsey.com

D. BAETZNER, A. ROMEO AND A.N. TIWARI
ETH Zurich, Laboratory for Solid State Physics, Thin Film Physics Group, Technopark, ETH Building, Technoparkstr. 1, CH-8005 Zurich, Switzerland

Abstract. CdTe layers have been grown on CdS layers to produce thin-film photovoltaic devices. Because of the large lattice mismatch of roughly 10%, CdTe and CdS can only be joined at the expense of a high density of misfit dislocations. Additionally, after deposition the CdTe layer contains submicrometer sized, [111] oriented, columnar grains with a high density of stacking faults and microtwins resulting in a poor electrical performance of the *p-n* junction. The performance of these cells can be improved by depositing a $CdCl_2$ layer on the CdTe absorber layer and subsequent annealing of the stack in air. This treatment induces interdiffusion of S and Te across the interface, which results in a better lattice match. During this anneal, CdTe is subject to grain growth, recovery and recrystallization. In samples annealed for different durations after different amounts of $CdCl_2$ were applied, grain growth is completed during the first minutes of annealing. Subsequent diffusion of Cl is detected along the CdTe grain boundaries. The presence of Cl enhances the recrystallization of the CdTe layer, starting from the CdTe surface, while recovery of the CdTe layer, mostly by the reduction of microtwins, takes place at the interface. The simultaneous occurrence of recrystallization and recovery leads to a preferred alignment of grain boundaries in CdTe parallel to the interface. Electron beam induced current measurements show the detrimental effect of these grain boundaries on the charge carrier collection efficiency of the cell. Based on these results, a modified growth procedure is proposed.

Keywords: solar cells, CdTe, $CdCl_2$, TEM

1. Introduction

Both its high absorption coefficient and its bandgap of 1.48 eV make CdTe a good absorber layer for photovolatic applications. As CdTe can be easily deposited by high growth-rate processes, it has a high potential as a thin-film solar cell absorber on an industrial level. Efficiencies of 7–10% have been obtained on large-area modules [1]. However, grain boundaries and structural defects both at the interface and in the bulk impose limitations of the efficiency of CdTe/CdS cells, since both reduce the photo current by recombination. An annealing treatment after deposition of $CdCl_2$ on the CdTe layer leads to grain growth, improves the cell efficiency and hence has been intensively studied, see e.g. [2]. However, little is known on the diffusion path of Cl in CdTe and how the simultaneous occurrence of grain growth, recovery and recrystallization influences the final texture of the CdTe absorber layer. Therefore transmission electron microscopy (TEM) has been used to obtain structural and chemical information on the changes induced by the $CdCl_2$ treatment.

*To whom all correspondence should be addressed. Now at: McKinsey & Co., Alpenstrasse 3, 8065 Zurich, Switzerland.

Table 1. Deposition and $CdCl_2$ treatment details of the samples.

Sample	$CdCl_2$/nm	time/min@temperature/°C	Deposition
1	0	as deposited	HVE
2	400	30@430 in air	HVE
3	150	30@430 in air	HVE
4	70	30@430 in air	HVE
5	0	30@430 in air	HVE
6	400	6@430 in air	HVE
7	400	11@430 in air	HVE
8	0	as deposited	CSS
9	100	15@420 in Ar + air	CSS

2. Experimental Details

A number of CdTe absorber layers were deposited by high-vacuum evaporation (HVE) as well as close-space sublimation (CSS). For HVE-grown cells, CdS layers approximately 700 nm thick were grown on SnO_X:F-coated soda lime glass (SLG) substrates at a substrate temperature of 150°C by use of HVE. A layer of CdTe of a thickness of 3 μm was deposited by means of HVE at a substrate temperature of 150 or 300°C. The CSS-grown cells consisted of a sputtered CdS layer of a thickness of 100 nm on SnO_X:F-covered SLG. The CdS layer was annealed in air at 500°C for 30 min prior to the CdTe deposition at 520°C. Both types of samples were submitted to different $CdCl_2$ treatments under the conditions listed in Table 1. From all stacks, cross sections were prepared by mechanical cutting and polishing, dimple grinding and ion milling. Electrical charging of the cross-sectional samples can occur, as the electrical conductivity of the SLG substrate is low. As the lateral resolution of long-term experiments to obtain EFTEM maps or EDS maps is clearly influenced by sample charging, some samples were covered with a thin, vapor-deposited carbon layer. Still, it was neccessary to regularly readjust microscope parameters, particularly during high-resolution TEM to prevent the effects of charging, as stigmation and beam deflection depend on the area investigated. The TEM studies were performed using a Philips CM30 electron microscope equipped with an energy-dispersive X-ray spectroscopy (EDS) system, and a Tecnai F30 electron microscope equipped with a Gatan imaging filter for energy-filtered TEM (EFTEM).

3. Experimental Results and Discussion

3.1. Structural Changes

An interface in as-deposited CdTe/CdS (HVE) is shown in the high-resolution micrograph of Fig. 1(A) with the CdTe layer in $[1\bar{1}0]$ and the CdS layer in $[2\bar{1}\bar{1}0]$ orientation. The CdTe grains grow epitaxially on the CdS grains, with the $\{111\}$ planes of CdTe parallel to the $\{0001\}$ planes of CdS. The polarity of the (0002)-layers of CdS is transferred across the interface to the (111)-planes of the CdTe layer. The lattice misfit

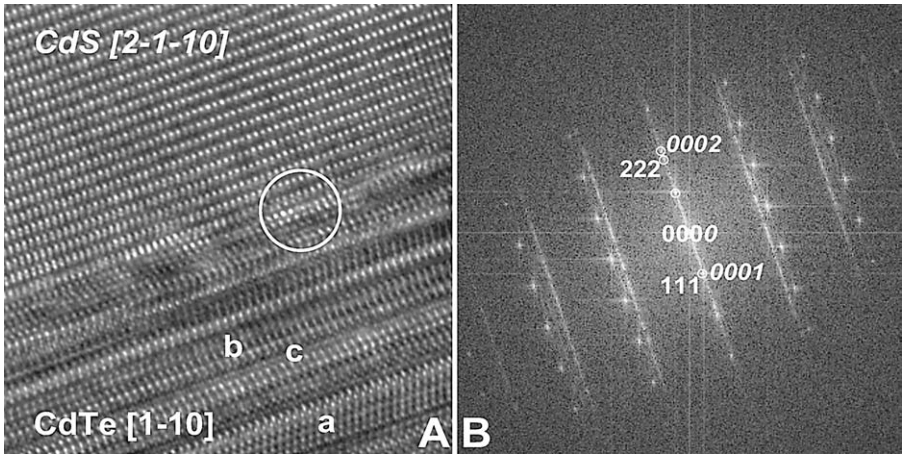

Figure 1. (A) High-resolution transmission electron micrographs of the CdTe/CdS interface after deposition. In the $[1\bar{1}0]$-oriented CdTe layer, the two twin variants of the cubic (a and b), the hexagonal stacking sequence (c) and a misfit dislocation (white circle) are marked. (B) Fourier transform of Fig. 1(A). Diffraction spots from the CdS layer are labeled in italics.

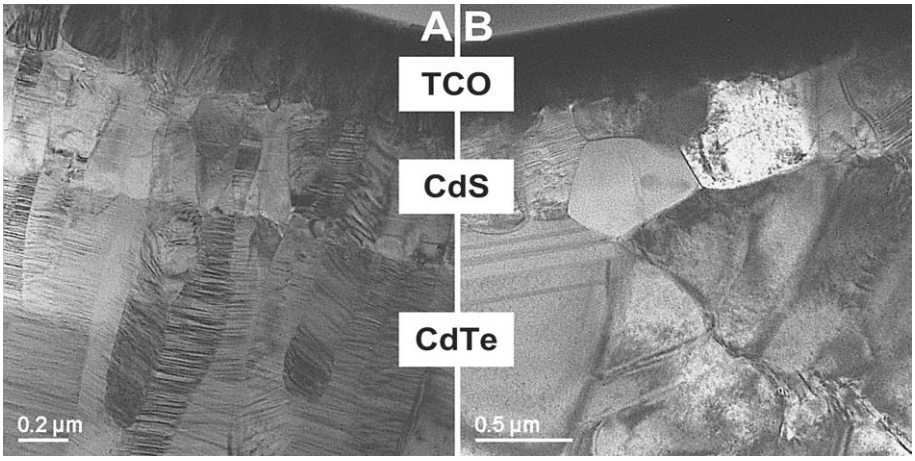

Figure 2. (A) A TEM micrograph in cross section of a CdTe/CdS cell after deposition. Both the columnar grain structure and the high density of twins in the CdTe layer are visible. (B) The same area after $CdCl_2$ treatment. Both, the CdTe and the CdS layers are characterized by grain growth (note the different scale bars), recovery and recrystallization. The CdTe/CdS interface exhibits grain coarsening.

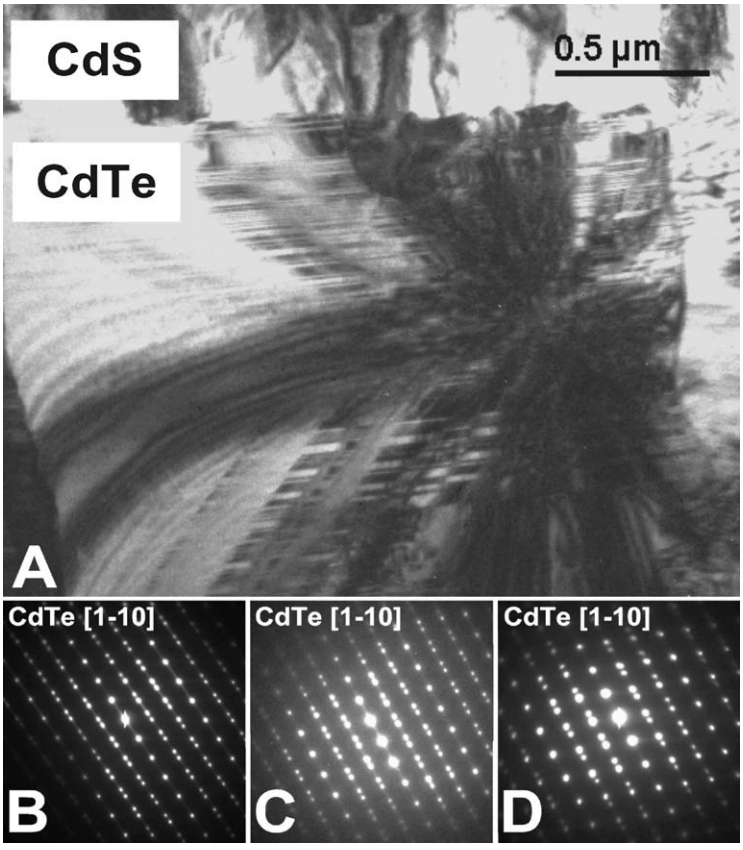

Figure 3. (A) Grain growth in a CdTe layer after 6 min of $CdCl_2$ treatment. No or little recovery has taken place yet. The CdTe layer shows extensive twinning in the SAED patterns, taken (B) 0.5, (C) 1.5 and (D) 3 μm away from the CdTe/CdS interface. All SAED were taken along the [1–10] zone axis.

of 10% between CdTe and CdS leads to misfit dislocations, one of which is marked in the micrograph. Both the orientational relationship and the lattice mismatch are reflected in the Fourier transform of the image of Fig. 1(A), as shown in Fig. 1(B). During the deposition of CdTe, both the low substrate temperature and the high deposition rate result in a reduced surface mobility of the Cd and Te atoms. In combination with the low stacking fault energy in CdTe, every few (111) layers a change in stacking sequence between one of the two twin variants (Fig. 1(A) a and b) or the energetically less favorable hexagonal stacking sequence (Fig. 1(A) c) occurs. The result is a high density of microtwins, which is reflected by the presence of streaks instead of well defined diffraction spots in Fig. 1(B). An overview of the CdTe/CdS interface and the CdTe absorber layer is given in Fig. 2(A). Both the microtwinning and the dependence of the CdTe grain size on the original grain size of the CdS layer and the columnar growth are visible. Figure 2(B) shows an overview of the cell after deposition of $CdCl_2$ on top of the CdTe layer and subsequent annealing. The CdTe and the CdS layers exhibit grain growth by a factor of 5–10 as well as recovery owing to the growth of one twin variant by the movement of partial dislocations. The texture of the CdTe layers before and after the $CdCl_2$ treatment has been studied by use of X-ray diffraction [5]. Recrystallization of CdTe indicated by the loss of [111] texture is found, which is enhanced in the presence of Cl during the annealing. Figure 3(A) is a micrograph taken from the CdTe/CdS interface of Sample 6. After 6 min of annealing, growth of the CdTe grains has already advanced throughout the absorber layer. While the large CdTe grain size indicates that grain growth is almost complete, selected area electron diffraction (SAED) patterns taken at different distances from the CdTe/CdS interface show still pronounced twinning of the material (s. Fig. 3(B), (C) and (D)). No or little recovery of the twinned CdTe layer is found. After 30 min of annealing, the CdTe absorber layer can be divided into two regions, as shown in Fig. 4. The region closer to the CdTe/CdS interface is still textured with preferred [111] orientation perpendicular to the interface. The CdTe grains show only few twin-domains resulting from recovery after 30 min of annealing by the movement of partial dislocations across the whole grain. Although the density of twins is reduced, they are still numerous and lead to the characteristic diffraction pattern. Figure 4(B) shows a representative SAED pattern from an area close to the interface along the $[1\bar{1}0]$ direction. The diffraction spots are indexed according to the twin variant and show that twins are present. The region away from the interface, which is closer to the CdTe surface, shows no preferred texture, and almost no twins are present. Hence, the SAED pattern in Fig. 4(C) shows well defined diffraction spots, originating from untwinned, $[1\bar{1}0]$-oriented CdTe. This indicates that recrystallization of the CdTe layer starts from the surface under the influence of $CdCl_2$. The driving force for recrystallization is the high density of twins in the as-deposited CdTe. Once this density is decreased by recovery, as for CdTe regions close to the interface, the recrystallization comes to a halt. The competition between recovery

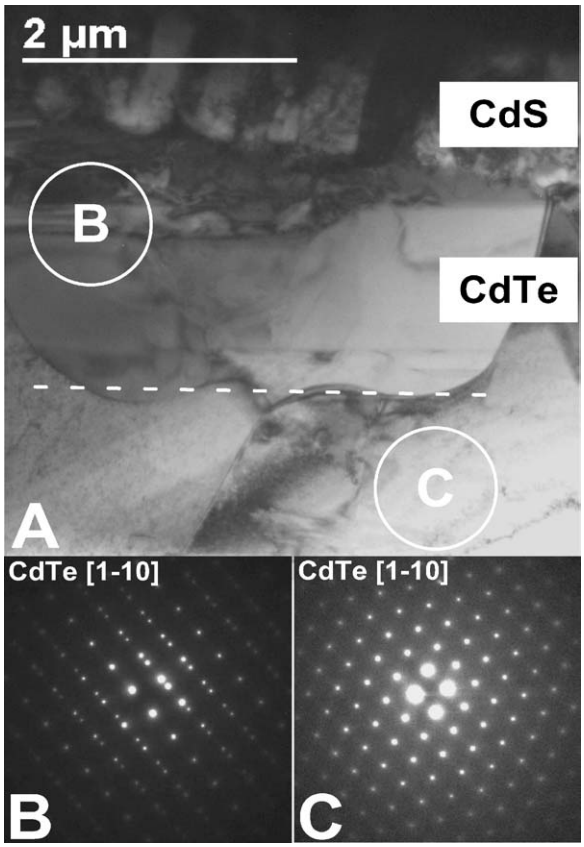

Figure 4. (A) A Grain boundary parallel to the CdTe/CdS interface as a result of the competition of recovery and recrystallization (dashed line). (B) Recovery in CdTe reduces the defect density, but twins with preferred [111] orientation with respect to the interface are still present as shown in the SAED pattern. (C) While recrystallization results in untwinned and randomly oriented CdTe grains. The areas selected by the selected area aperture for the electron diffraction shown in (B) and (C) are marked by the white circles and indexed in Fig. 4(A).

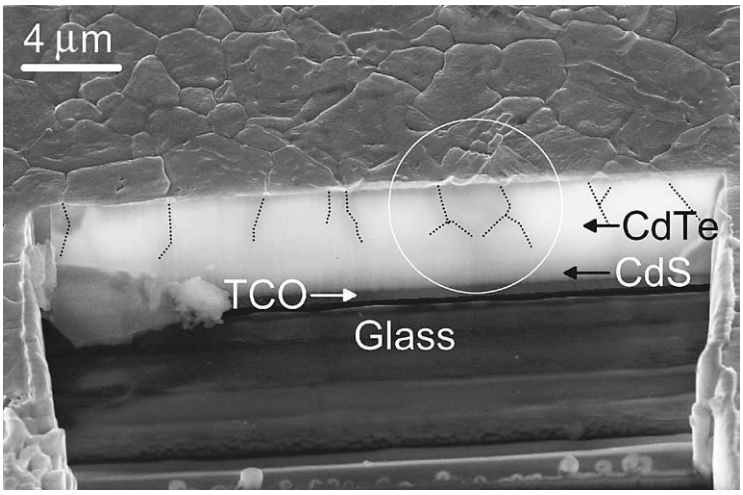

Figure 5. A superposition of a secondary electron image of a CdTe/CdS cross section taken, with a scanning electron microscope, and the corresponding electron-beam induced current signal. Dark regions are electrically less efficient. The grain boundaries in the CdTe layer are marked. Note the reduced electrical activity in the area isolated from the interface by horizontal grain boundaries (white circle).

close to the interface and recrystallization at the CdTe surface leads to a preferred alignment of grain boundaries parallel to the interface. These grain boundaries passivate regions of the CdTe absorber, as current transport is reduced by charge carrier recombination. Figure 5 shows an electron beam induced current (EBIC) image of the absorber layer. The cross section was cut with a focused ion beam to avoid topographical effects of surface roughness on the EBIC measurements. After the EBIC image had been taken, the grain boundaries in the CdTe layer were made visible by etching with nitric phosphoric acid, an agent that etches preferentially at grain boundaries. In Fig. 5, a superposition of the EBIC signal and the corresponding scanning electron micrograph of the region is shown. Regions of poor electrical performance (e.g. low collection efficiency through carrier recombination) appear darker. These regions of poor electrical performance coincide with regions that are separated from the interface by grain boundaries parallel to the interface. The grain boundaries are additionally marked in Fig. 5.

3.2. Chemical Changes

To assess and quantify the diffusion of S and Te across the CdTe/CdS interface and its dependence on the $CdCl_2$ treatment, samples were investigated by EDS mapping. The interface was aligned parallel to the electron beam. Thickness effects were eliminated by taking ratios of signals rather than their absolute values. The composition across the interface is best presented as a linescan taken perpendicular to the interface and averaged over a lateral width of 100 nm. All intensities measured were calibrated to concentrations using standards of $Cd_{50}S_5Te_{45}$ and $Cd_{50}S_{45}Te_5$ polycrystals. Figure 6 shows a comparison of the concentration of S in untreated CdTe layers deposited by CSS and HVE. For all samples, the S concentration in the CdTe layers is well below 1.5 at.%, at and beyond the interface. Neither the growth process nor the temperature of deposition had a strong influence on the diffusion of S. For all samples, $CdCl_2$ treatments of varying extent were applied and again, the S concentration was measured. Figure 6 also shows results for a cell grown with HVE at 300°C. With increasing amounts of $CdCl_2$ applied, a concentration profile of S develops in the CdTe absorber layer. Concentrations of S of up to 6 at.% at the interface and less than 1.5 at.% about 1.5 μm away from the interface were observed. The phase diagram of CdS-CdTe [4] does not predict a content of S of more than 6.5 at.% for a CdS_XTe_{1-X} layer without phase separation. This is in accordance with the absence of any S segregation and the values found. The diffusion of S causes a reduction in thickness of the CdS layer, e.g. by approximatly 100 nm for the CdS layer of HVE-deposited samples treated with 300 nm of $CdCl_2$. As a result of this reduction, in combination with surface roughening during the recrystallization of the CdS layer (compare Fig. 2(A) and (B)), HVE-grown CdS layers thinner

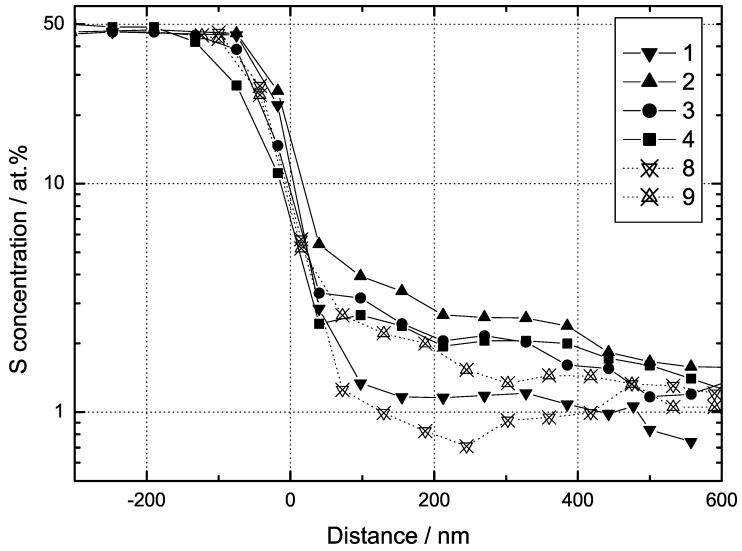

Figure 6. Concentration profiles of sulfur across the CdTe/CdS interface for both high vacuum evaporation and close-space sublimation grown cells after deposition and after treatment with different amounts of $CdCl_2$ (s. Table 1).

than 200 nm form CdS-free regions across the interface. Thereby, electrical shunts are produced through a direct contact between the *p*-conducting CdTe and the TCO. One of these shunts is shown in Fig. 7, a sulfur-EFTEM map of the interface. Bright regions with high S content mark the presence of CdS. The formation of these shunts limits the possible minimum thickness of HVE-grown CdS layers. However, a thin CdS layer is of crucial importance for the cell performance, as light absorption increases with the thickness of the layer. In particular, photons of a wave length smaller than 600 nm are absorbed and hence the number of charge carriers generated in the CdTe absorber layer is reduced [6]. The CdS layer in cells grown by CSS had been recrystallized by annealing prior to the CdTe deposition. In these cells, S diffusion is reduced (s. Fig. 6).

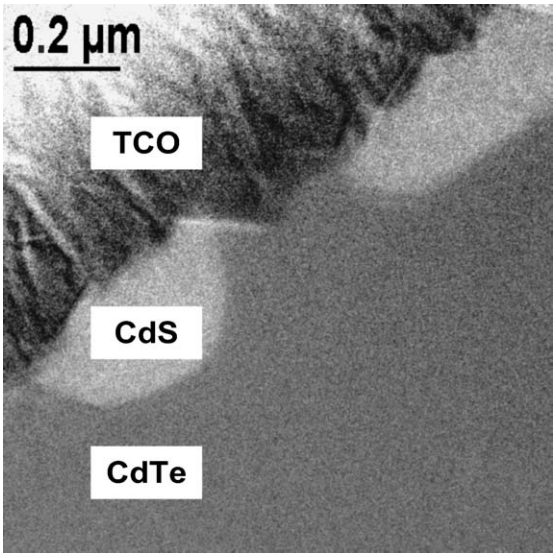

Figure 7. Energy-filtered transmission electron micrograph of a 200 nm thick CdS layer after $CdCl_2$ treatment taken at the S L-edge. The chemical mapping reveals CdS free areas that lead to shunts between the CdTe and the TCO.

3.3. The Role of Chlorine

As the recrystallization of the CdTe layer is pronounced in the presence of Cl, EFTEM was used to locate the Cl after the annealing process. From the evolution of X-ray diffraction line profiles measured for $CdCl_2$-treated CdTe films, the diffusion coefficient of Cl in CdTe for grain boundaries is known to be five orders of magnitude larger than the diffusion coefficient of Cl in bulk CdTe [5]. Therefore, Cl diffusion is expected to be dominated by grain boundary diffusion. The shortest annealing times (Sample 7) yield no detectable accumulation of Cl in the CdTe layer. Only with increasing annealing time, the amount of Cl diffused along CdTe grain boundaries can be detected (s. Fig. 8). As at this point the grain growth is essentially complete,

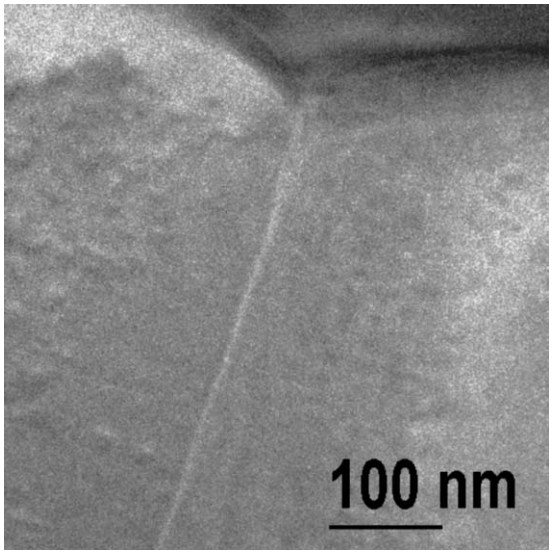

Figure 8. An energy-filtered TEM map of a grain boundary running perpendicular to the CdTe surface, taken at the Cl L-edge. The $CdCl_2$ treatment was stopped after 11 min. Segregation of Cl along CdTe grain boundaries is revealed.

the grain boundaries can be considered stable for the Cl diffusion. Further annealing evaporates the $CdCl_2$ layer from the CdTe surface and, in the absence of a Cl source, Cl diffuses from the grain boundaries into the bulk CdTe. Excess Cl is found to segregate at the CdTe/CdS interface. An EDS map of the interface region is shown in Fig. 9. Regions with increased Cl as well as O and Te contents are visible. While the Cd concentration across the interface remains unchanged, regions with Cl, Te and O segregation are primarily found along CdS grain boundaries, with a corresponding depletion of S. The segregated elements seem to replace the missing sulfur. A precise determination of the concentrations is rather difficult owing to the large number of elements. However, the simultaneous presence of Cd, Cl, Te and O is in agreement with the chemical reaction at 430°C proposed by McCandless [7].

$$CdCl_2(\text{solid}) + O_2(\text{gas}) + CdTe(\text{solid}) \Leftrightarrow TeCl_2(\text{gas}) + 2CdO(\text{solid}) \quad (1)$$

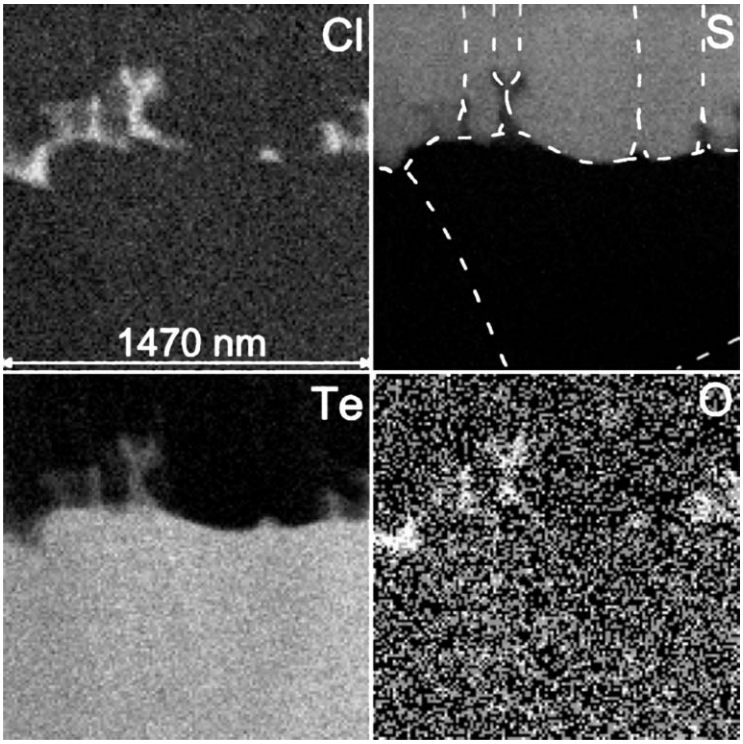

Figure 9. Energy dispersive X-ray spectroscopy mappings of the CdTe/CdS interfacial region. At the interface and in particular along the CdS grain boundaries the concentration of Te, Cl and O is higher while the grain boundaries are depleted of S. In the S map, the grains are outlined along the boundaries for clarity.

The presence of $TeCl_2$ vapor would increase the surface mobility of both Cd and Te atoms and hence promote the recrystallization of CdTe.

4. Conclusions

CdTe/CdS thin-film solar cells have been investigated with a focus on structural and chemical changes induced during annealing of the cells under the influence of Cl. Although the CdTe layer grows quasi-epitaxially on CdS, the CdTe/CdS interface is imperfect owing to the lattice mismatch between CdTe and CdS. The CdTe absorber layer is of poor crystal quality as it contains numerous microtwins and small, [111] textured, columnar grains. The grain size in the CdTe layer is determined by the CdS grain size at the interface. Therefore, an annealing after CdS deposition prior to CdTe deposition, inducing grain growth in the CdS layer could lead to larger CdTe grains. During the first minutes of annealing under Cl influence, grain growth is the dominating mechanism in the restructuring of the CdTe layer. It is presumably driven by both, the difference in the density of structural defects and a high grain boundary energy. The grain diameter in the CdTe layer increases by a factor of 5 to 10 while grains retain their columnar shape and a high density of twins. Continuous annealing results in recovery of the CdTe microstructure close to the interface, while the volume closer to the CdTe surface shows recrystallization driven by the high density of twins. The recrystallization is enhanced in the presence of Cl. Cl is shown to migrate along CdTe grain boundaries towards the interface. Further investigations are planned to decide whether the mechanism described by Eq. (1), which was derived from the analysis of Cl, Te and O segregation at the interface, explains the influence of Cl. Another explanation could be pinning of partial dislocations by Cl and hence a slowing-down of the recovery, until recrystallization sets in. As the recovery of CdTe is more advanced closer to the interface, the recrystallization comes to a halt. This results in the formation of grain boundaries parallel to the interface, which are detrimental to the cells performance as shown by EBIC mesurements. During the annealing, S diffuses from the CdS layer into the CdTe layer. The extent of diffusion depends on the amount of $CdCl_2$ applied. The consumption of CdS due to diffusion of S leads to the formation of shunts across the interface. In CSS grown CdTe, grown on CdS that was annealed before the CdTe was deposited, diffusion of S into CdTe layers is less pronounced. This annealing process may make it possible to work with thinner CdS layers without shunting in cells produced by HVE deposition of CdTe.

Acknowledgments

The authors are very grateful to E. Fischer, ETH Zurich, for the preparation of the $Cd_{50}S_5Te_{45}$ alloy and to N. Romeo, University of Parma, for the CSS-grown cells.

References

1. M. Harr and D. Bonnet, in *Proceedings of the 17th European Photovoltaic Solar Energy Conference and Exhibition*, edited by B. McNelis, W. Pals, H. Ossenbrink, and P. Helm (WIP-Munich and ETA-Florence, Munich, 2001), p. 1001.
2. K. Durose, P.R. Edwards, and D.P. Halliday, Journal of Crystal Growth **197**, 733 (1999).
3. H.R. Moutinho, M.M. Al-Jassim, D.H. Levi, P.C. Dippo, and L.L. Kazmerski, J. Vac. Sci. Technol. A **16**, 1251 (1998).
4. D.W. Lane, G.J. Conibeer, D.A. Wood, K.D. Rogers, P. Capper, S. Romani, and S. Hearne, Journal of Crystal Growth **197**, 743 (1999).
5. B.E. McCandless and R.W. Birkmire, in *Proceedings of the 16th European Photovoltaic Solar Energy Conference and Exhibition*, edited by H. Scheer, B. McNelis, W. Pals, H. Ossenbrink, and P. Helm (James & James, London, 2000), p. 349.
6. D. Baetzner, G. Angostinelli, A. Romeo, H. Zogg, and A.N. Tiwari, in *II-VI Compound Semiconductor Photovoltaic Materials*, edited by R. Noufi, R.W. Birkmire, D. Lincot, and H.W. Schock (Material Research Society, Warrendale, 2001), H5.17.
7. B.E. McCandless, in *II-VI Compound Semiconductor Photovoltaic Materials*, edited by R. Noufi, R.W. Birkmire, D. Lincot, and H.W. Schock (Material Research Society, Warrendale, 2001) H1.6.1.